Sanchez-Gonzalez, E.; Pinilla-Cienfuegos, E.; Borrero-Lopez, O.; Rodriguez-Rojas, F.; Guiberteau, F. (2020). Contact damage of human dental enamel under cyclic axial loading with abrasive particles. Journal of the Mechanical Behavior of Biomedical Materials. 102. https://doi.org/10.1016/j.jmbbm.2019.103512

CONTACT DAMAGE OF HUMAN DENTAL ENAMEL UNDER CYCLIC AXIAL LOADING WITH ABRASIVE PARTICLES

Estibaliz Sanchez-Gonzalez[a♣], Elena Pinilla-Cienfuegos[b♣], Oscar Borrero-Lopez,[a]*, Fernando Rodríguez-Rojas[a], and Fernando Guiberteau[a]

[a] *Departamento de Ingeniería Mecánica, Energética y de los Materiales, Universidad de Extremadura, 06006 Badajoz, Spain*
[b] *Valencia Nanophotonics Technology Center (NTC), Universitat Politècnica de València, Camí de Vera, s/n, 46022 Valencia, Spain*

♣Both authors contributed equally to this work

**Email:* oborlop@unex.es

Abstract

The damage to human dental enamel under cyclic, axial contacts in a silica particle medium is investigated. It is found that such damage is hierarchical, affecting different length-scales of the enamel structure. At the contact surface, it consists of micron-sized defects, with an attendant increase of surface roughness due to microindentation of the abrasive particles. Below the surface, demineralization of the enamel is observed, which is attributable to inelastic processes at the nanoscale. Axial-only contacts in particulate media result in negligible wear at the macroscopic scale, but may degrade the fracture strength. Potential implications of these results in the fields of dentistry and biology are discussed.

Keywords: Enamel; Microstructure; Hertzian contact; Abrasive particles

1. Introduction

Mastication is a complex combination of normal (axial) and lateral (sliding) forces. The prevalence of an axial or sliding component largely depends on diet. In particular, it is assumed that hard foods (*e.g.*, nuts) are broken down using axial forces, while chewing softer/tougher foods (*e.g.*, vegetable matter, meat) also requires shear forces (sliding) [1, 2].

Micrometer-scale silica particles in the environment (exogenous, *e.g.*, dust [3]) or in the food source (endogenous, *e.g.*, phytoliths [4]) are of great importance in dentistry and paleodontology because when they incorporate into the bolus they have the potential to damage dental enamel and accelerate tooth wear. At the microscopic level, it is well-documented that abrasive particles trapped between contacting teeth result in characteristic microwear signals: pits (axial contacts), and scratches (sliding contacts) [5-9]. The cumulative effect of microwear events results in enamel macrowear—a severe wear rate may in turn result in decreased tooth lifetime [10]. Previous studies on the role of particles in enamel macrowear have focused mainly on sliding contacts. It has been shown that adding silica abrasives under a sliding contact can increase enamel macrowear by orders of magnitude, from mild to severe, with respect to a particle-free contact [11]. The wear rate is largely independent of particle concentration, but it may decrease for higher vol% particles if there occurs a transition in the microwear mode from microcracking to microplasticity [12].

Despite having been extensively researched in the fields of ceramic materials [13-19] and coatings [20, 21], the effects of cyclic, axial-only contacts on the damage and wear of dental enamel are less well-documented. A study applying a small number of cycles with a sharp Berkovich tip in a nanoindenter showed different fatigue responses in occlusal and axial sections of enamel [22] . More recent work has found that enamel is also subject to fatigue from larger, blunt contacts, even at relatively low loads, due to the

nucleation and propagation of ring and radial cracks [23]. Moreover, preliminary studies of cyclic, axial contacts with particles have established the fundamental differences in the nature of the surface damage at the microscopic scale (pits) with respect to sliding contacts (scratches) [6]. However, important issues remain to be addressed. In particular, do cyclic, axial-only contacts in particulate media result in enamel macrowear? If so, is it mild or severe? Is the damage comparable with what occurs in sliding contacts?

The present paper seeks to address these issues by simulating axial-only contacts with suspensions of micrometric size, abrasive silica third body particles (representative of exogenous/endogenous grit) on human enamel specimens, and subsequently investigating the ensuing damage at the macro- and micro-scales using a suite of structural characterization techniques (optical and scanning electron microscopy, Optical Coherence Tomography (OCT), and Raman spectroscopy). The advantage of these techniques is that they are non-destructive, and allow surface and sub-surface examinations while avoiding spurious damage introduced on sectioning by more conventional mechanical (*e.g.*, saw) or electronic (*e.g.*, laser, ion beam) cutting techniques. The damage at the macro-scale is quantified and used to make predictions of tooth lifetime. The results are expected to be important in the context of the influence of diet on tooth damage, which has direct implications in dentistry and evolutionary biology.

2. Materials and methods

The collaborating dental clinic supplied dental samples, namely impacted molars (*i.e.*, free of damage) of healthy appearance, collected from young adult patients. Tooth enamel specimens were fabricated from the supplied extracted human molars. In particular, flat slices parallel to occlusal surfaces were cut and polished to 1 µm finish using a conventional ceramographic routine. Preliminary Vickers microindentation tests

(applied load 200 g) were conducted on the enamel specimens, and only those of hardness 3.5-4.5 GPa, characteristic of sound enamel [24], were finally selected for the study in order to ensure that the samples were comparable. Cyclic Hertzian tests were subsequently conducted on polished, occlusal molar surfaces using a silicon nitride sphere of radius 6.35 mm (Cerbec NBD 200, CoorsTek, Golden, CO), as shown schematically in Fig. 1. Silicon nitride was chosen as a contact material because it is harder and stiffer than enamel, in order to ensure that damage occurs only in the latter. A suspension of 0.5 vol% hard, angular silica particles of mean size 20 μm (A. Anglada, Zaragoza, Spain) in distilled water was introduced between contact sphere and the specimen (Fig. 1). A low concentration of micrometric silica particles is expected to be representative of exogenous and endogenous grit. The normal load applied was P=30 N, which results in a macroscopic contact pressure within the nominal elastic range of enamel [10]. Tests were conducted in a universal test machine (5535, Instron, Canton, MA) at a crosshead speed of 6 mm/min, so as to simulate realistic chewing motion conditions. In between contacts, the sphere is lifted approximately 3 mm from the enamel surface. The numbers of total contact cycles tested were 500, 1000, 1500 and 2000. Three different tooth specimens were tested in each case, giving a total of 12 tests.

The surface of the specimens after testing was inspected by optical (Epiphot 300, Nikon, Tokyo, Japan) and scanning electron (S-3600N, Hitachi, Japan) microscopy, and by contact profilometry (Dektak 150 Surface Profiler, Veeco Instruments, Plainiview, NY). The scanning electron microscopy (SEM) images were obtained using secondary electrons (thermionic gun) accelerated at 5-15 kV, under $1.5 \cdot 10^{-3}$ Pa vacuum pumped at a relatively low speed to avoid enamel cracking due to dehydration. The low conductivity of enamel requires surface metallization (gold coating) prior to observation. Contact profilometry measurements extended across the entire scar diameter (up to ≈1 mm), with a maximum depth of ≈1 μm. The volume of each wear scar was estimated by substituting

in the equation of a spherical cap ($V=(\pi h^2/3)\cdot(3R-h)$) the depth of the scar measured from the profile (h), and the radius of curvature (R) obtained by fitting a circle to its profile.

In order to investigate possible damage under the surface, three selected specimens were also inspected by Optical Coherence Tomography (OCT) (Callisto 930 nm OCT Imaging System, Thorlabs, USA) and Raman spectroscopy (Raman/AFM alpha300 RA, Witec, Germany). While Raman is confined to the region at the surface and immediately below, OCT probes a region extending deeper under the surface. In particular, Spectral Domain OCT (SD-OCT) B-scan images (1 mm width, 1.68 mm depth, 3.58 μm × 2.22 μm pixel size and 0.67 s acquisition time inside the scar; and 1.5 mm width, 1.68 mm depth, 3.3 μm × 3.29 μm pixel size and 0.67 s acquisition time outside the scar) were collected at 930 nm wavelength. In all cases, the sample was slightly tilted with respect to the B-scan axis to avoid imaging artifacts (nonlinear response of the spectrometer). High resolution Raman spectral imaging (lens magnification ×50, laser wavelength 532 nm, grating 600 l/mm, spectral resolution 2-3 cm^{-1} per CCD pixel, lateral resolution ≈500 nm, axial resolution (confocal) ≈3μm) was performed at the edge of the contact zone. Raman spectra at 532 nm excitation wavelength were collected at every measurement point (300 × 300 points, 0.03519 s integration time) and therefore, in one single Raman image (100 μm × 100 μm scan), multiple mineral species (each represented by its own Raman spectrum) could be acquired. In particular, a Raman image was generated from changes in one specific Raman peak (peak intensity). For the confocal Raman imaging, stacking mode was used and layers of 80 μm × 80 μm area with 160 × 160 points, 0.03615 s integration time, were scanned at different depths, up to 8 μm.

The principal advantage of the OCT and Raman techniques for the present study is that they are non-destructive. Thus, they allow sub-surface examination of cross-sectional structure and damage while avoiding the distortions that are typically introduced by more conventional sectioning techniques, such as the microcracks

generated during mechanical cutting/grinding, and the welding or ion implantation caused by high energy laser or ion beams. Moreover, the Raman spectroscopy can reveal the microstructure of the enamel, which is otherwise difficult to image with other non-invasive techniques such as optical or scanning electron microscopy.

3. Results

Images (optical micrographs) of the scars on enamel occlusal surfaces, obtained after Hertzian tests in water with particles under different contact cycles, are shown in Fig. 2. The impressions are near circular, with irregular edges compared to particle-free, ideal Hertzian scars (*i.e.*, regular circles conforming to the edge of the elastically deformed contacting sphere [25]), due to the presence of abrasives under the contact. The diameter of the scars is observed to increase with the number of contact cycles, ~~although significantly less so than in the case of a sliding contact [12]~~. Some amount of debris can also be observed, adhered to the surface near the perimeter of the contact zones —after testing, and prior to observation, enamel surfaces were only gently cleaned with distilled water to avoid introducing further damage.

Representative cross-sectional profiles of the scars are shown in Fig. 3. Three main observations can be made. First, the scars produced by repetitive axial contacts are shallow, with depths of the order of < 1μm, and diameters of the order of < 1 mm—horizontal profiles indicate the end of the scars. Second, the profiles of these scars are very irregular and noisy, with steps inside the scars with heights of ~10's of nm. ~~This contrasts with the smooth and polished profiles of significantly larger depth (in the order of ~10's of μm) produced by sliding contacts [11]~~. And third, consistent with the optical microscopy observations, both the width and depth of the scars are seen to increase with increasing number of contact cycles.

Intermediate and high magnification details of the damage inside the scars can be observed in Fig. 4. As reported before, axial contacts produce characteristic microscopic markings in the form of pits [6]. The pits observed have widths between 1 and 20 μm, approximately, which suggests that they are formed by the repeated microindentation of the abrasive particles under the contact in different parts of the enamel microstructure. The larger and wider pits with smoother surfaces (pointed to by white arrows in Fig. 4(B)) are characteristic of a predominantly brittle response (*i.e.*, lateral crack chipping), with deeper zones within corresponding to the steps observed in the profilometry images. In contrast, the smaller and sharper pits (pointed to by black arrows in Fig. 4(B)) suggest a predominantly ductile response, and are thus attributable to sub-threshold microindentation on softer parts of the microstructure [5, 12]. Large-scale cracking due to dehydration of the enamel under the vacuum conditions inside the SEM chamber was not observed in the examined specimens.

The presence of sub-surface damage can be investigated by means of OCT and Raman spectroscopy. The OCT technique has recently been used in dentistry due to its capability for real-time, sub-surface imaging of the internal tooth structure at high spatial resolution [26]. Fig. 5(A) shows a low magnification optical image (stereoscope) of the surface of one sample after 500 contact cycles, where the contact zone is visible and appears markedly brighter than the rest of the enamel surface. Representative OCT images of the cross-section outside the contact as control (blue arrow in Fig. 5(A)) and under the contact (red arrow in Fig. 5(A)) are shown in Figs. 5(B) and 5(C), respectively. A uniform region of relatively high brightness is observed everywhere under the surface, which is attributed to the increased light scattering in demineralized tissue [27, 28]. However, comparison between the cross-sections under and outside the scar reveals a region of increased brightness directly under the contact, marked by the black arrows in Fig. 5(C) (in the optical image it is observed from above due to the enamel's translucency). This region extends up to ≈0.6 mm below the surface, and suggests a

larger extent of sub-surface demineralization under the scar. Damage of the same nature is expected to be also present after tests at higher contact cycles.

Further evidence of enamel demineralization under the contact can be obtained from Raman spectroscopy, by analyzing the characteristic peaks of hydroxyapatite ($Ca_{10}(PO_4)_6(OH)_2$), the main mineral component of enamel [29]. In particular, Fig. 6 shows an optical image (Fig. 6(A)), and two Raman images (Figs. 6(B) and (C)) of the same area, acquired at the edge of a scar after 500 cycles. The Raman images were generated from near-surface measurements of the intensities of the (1040±10 cm^{-1}) and (962±10 cm^{-1}) phosphate (PO_4) Raman peaks, which correspond to the ν_3 asymmetric stretching modes and the ν_1 symmetric stretching mode of PO_4, respectively [30]. The image obtained from the (1040±10 cm^{-1}) peak (Fig. 6(B)) exposes the mineral rods in the enamel, and reveals that, past the surface damage created by the abrasives, the microstructure does not get distorted significantly inside the scars. On the other hand, the image obtained from the (962±10 cm^{-1}) peak (Fig. 6(C)), which is the sharpest and most intense band of the enamel [30], shows a clear contrast between the inside (darker) and outside (lighter) of the contact region. This contrast is attributable to differences in the vibrational spectra resulting from differences in the mineral content, with darker regions indicating a lower mineral content [29]. Indeed, the comparison of Raman spectra collected inside and outside the scar (the latter as control) in Fig. 7 shows a significantly lower intensity of the peak at (963 ± 3 cm^{-1}) inside (red line in Fig. 7), thereby confirming the relative demineralization of the enamel immediately under the contact with respect to fresh enamel. Confocal images formed from measurements of the intensities of the (960 ± 30) cm^{-1} peak in stacking mode at different depths (Fig. 8) also confirm that the demineralization extends below the contact surface. Indeed, the contrast between inside (darker) and outside (brighter) scars after 500 and 2000 cycles is maintained as the depth (distance from the surface) increases from 0 μm to 6 μm in the 500 cycles sample, and from 0 μm to 8 μm in the 2000 cycles sample. This indicates sub-

surface demineralization under the contact regions, which is in agreement with the OCT measurements.

4. Discussion

Human enamel has a multi-scale, hierarchical structure [31]. At the microstructural scale it consists of mostly mineral (relatively hard) rods of diameter ~5 μm, oriented perpendicularly to the occlusal surface, separated by thin, protein-rich (relatively soft) sheaths, as revealed in Fig. 6(B). The nanostructure of individual rods consists of elongated, hexagonal hydroxyapatite crystals (lengths ≈70 nm, widths ≈30 nm) aligned parallel to the rod axis and separated by a thin (1-2 nm) protein layer [32].

The results in Section 3 indicate that cyclic, axial contacts with abrasive particles introduce damage in the enamel at both micro- and nano-structural levels. Firstly, there is the near-surface damage within the contact area produced by particle microindentation events, at the microstructural scale. Indeed, the larger and smaller pits observed in Fig. 4 are attributable to microindentation events primarily on harder rods and softer sheaths, respectively. And secondly, there is an apparent demineralization of a region deeper below the contact. The shape of the demineralized region observed by OCT (Fig. 5(C)) roughly coincides with the region of maximum shear stresses in an ideal Hertzian contact, and resembles a quasiplastic zone observed in coarse-grain ceramics [25].

It is important to note that this sub-surface damage is generated at relatively low macro-contact pressures of < 1 GPa, as estimated from the size of the initial contact at load P= 30N. Such pressures are well below $H/3$ for enamel (≈1.3-1.5 GPa), which is widely used as a first estimate of the yield strength from Hertzian tests [33, 34]. Indeed, as seen in Fig. 6(B), it is insufficient to cause noticeable distortion of the rod structure at the microstructural level. Without particles in the test media, the contact does not produce

a scar that can be detected by optical microscopy. However, at the nanoscale, inelastic processes in enamel (*i.e.*, within individual rods) have been reported to start at lower pressures [35, 36]. Even under relatively low stresses, the softer protein undergoes large shear deformations, resulting in an inelastic response [36, 37]. Jia and Xuan [22] noted the partial interface de-bonding between crystals. Thinning or failure of the protein layer brings hydroxyapatite crystals into closer contact. Subsequent cyclic loading results in relative sliding of adjacent crystals [36]. We posit that the greater internal friction of such sliding contacts [14], resulting from the inelastic thinning/failure of the protein layer, may be responsible for the apparent loss of mineral content. Although direct evidence of this in enamel is only possible by high resolution transmission microscopy of extreme difficulty, a parallel can be drawn with the frictional degradation of grain boundaries which has been observed in thin films with a columnar microstructure, analogous to that of enamel, under cyclic loading with a spherical indenter [20].

In order to assess whether or not the damage at the microscopic level results in significant damage at the macroscopic scale, the volume of the scars produced in the axial contacts was quantified from their profiles (Fig. 3). Figure 9(A) shows the evolution of the scar volume as a function of the number of contact cycles. Such volumes are significantly lower (by an order of magnitude) than the ones reported in contacts in similar loading conditions involving a frictional force (*i.e.*, sliding) [12]. The small amount of wear is due the abrasive particles dislodging of material from the surface, as seen in Fig. 4. Moreover, the rate of material removal is also very low: from a linear fit to the data in Fig. 9(A), a value of $\approx 1 \cdot 10^{-7}$ mm^3/axial cycle is calculated. Comparison with a sliding contact is not straightforward, as the length of an equivalent sliding contact is somewhat arbitrary. In earlier work, $L=2r$ was employed as the length of one full lateral/sliding chewing cycle, with r being the tooth radius. Taking a value of $r=5$ mm [10, 11], a material removal rate of $\approx 3 \cdot 10^{-6}$ mm^3/sliding cycle is calculated from sliding data in comparable conditions (30 N normal load, 0.5 vol% quartz abrasives,

corresponding to a wear coefficient $K=4\cdot10^{-5}$, simulating tooth grinding in bruxers) [12]. The large differences in wear volumes and rates between axial and sliding contacts can be visualized in Fig. 9(B).

From the rates of material removal calculated above, the critical number of chewing cycles required to remove the enamel completely (N_C, which is indicative of tooth lifetime) can then be estimated. Considering a simplistic model of a tooth as a cylinder of radius 5 mm, with an enamel cap of thickness 1.5 mm [10, 11] , the critical number of axial cycles obtained is $N_C=1.2\cdot10^9$. For the same tooth under sliding contact, the critical number of sliding cycles is estimated to be $N_C=4\cdot10^7$. Against a benchmark of 10^6 contacts/year [38], the N_C values translate into tooth lifetimes of 40 years (sliding), and 10^3 years (axial). These figures reinforce the assertion that tooth wear is only a concern in contacts with a sliding component.

The results obtained in this work reveal that the damage introduced to enamel by repetitive, axial contacts with abrasives is multi-faceted, and differs profoundly from what is typically observed in sliding contacts. In particular, axial-only contacts result in negligible (but not zero) wear at the macroscopic scale, with rates of material removal at least one order of magnitude lower than analogous sliding contacts. This, in turn, translates into significantly longer estimated tooth lifetimes in a purely axial contact, compared to pure sliding. However, our results show that axial contacts result in additional forms of damage at smaller length-scales, even at low loads, which may also affect the tooth lifetime. First, the microindentation damage introduced by the abrasive particles creates micron-sized defects, localized on the contact surface, which increase the roughness. This contrasts with the smooth and polished profiles of significantly larger depth (in the order of ~10's of μm) produced by sliding contacts [11]. And second, cyclic axial contacts result in demineralization of the enamel under the contact, seemingly as result of inelastic processes at the nanoscale. The damage modes and material removal

rates are expected to be largely independent of particle concentration, at least in the low concentration range 0.1-5 vol% [12].

The main implications of the present results are in the fields of dentistry and evolutionary biology. In dentistry, severe tooth wear has traditionally been related to such disorders as bruxism (tooth grinding), characterized by the application of abnormally high lateral jaw forces [39]. Our conclusion that predominantly lateral forces result in enamel wear agrees with the previous observation. The negative effects of axial mastication, which is associated with hard food items, lie in tooth fracture, rather than wear. In particular, a blunt, axial contact may introduce defects on the surface (especially in particulate media), and demineralize the enamel below. The former requires lower stress for crack propagation than the natural flaws in enamel, and the latter worsens the material mechanical properties [24]. Within the framework of fracture mechanics, both may result in strength degradation, and increase the probability of failure at a relatively low load [40]. This appears to be consistent with evidence in the fossil record showing relatively more tooth chipping in *Paranthropus robustus* (hard food diet, predominantly axial bite) than in *Paranthropus boisei* (consumer of larger quantities soft food, lateral bite) [41]. Additionally, for a higher number of contact cycles, axial contacts have been shown to result in fatigue [23], although the combined effects of demineralization and fatigue remain to be investigated. Finally, the greater roughness resulting from the introduction of surface defects can increase the wear caused to the opposing tooth (antagonist wear), as evidenced by *in-vitro* and *in-vivo* experiments with dental prostheses [42, 43].

5. Conclusions

We have studied the damage of human dental enamel under cyclic, axial contacts in a silica particle medium, using Hertzian indentation and a suite of non-destructive techniques for structural characterization at different length scales. Based on the results and analyses, the following conclusions can be drawn:

1. At the contact surface, the damage consists of micron-sized defects, due to microindentation of the abrasive particles.
2. The axial forces cause demineralization of the enamel below the surface, even at low contact cycles, as confirmed by OCT, Raman spectroscopy and confocal Raman measurements. ~~which is attributable to inelastic processes within the enamel rods at the nanoscale~~.
3. Axial-only contacts in particulate media produce shallow scars, which result in negligible enamel wear at the macroscopic scale. ~~but the surface defects and demineralization introduced may degrade the fracture strength~~.

Acknowledgements

The authors wish to thank Dr. Florencio Monje Gil for kindly providing tooth specimens from his clinic (CICOM, Centro de Implantología Cirugía Oral y Maxilofacial, Badajoz, Spain). Fruitful discussions with Dr. Brian Lawn (National Institute of Standards and Technology, NIST, MD), Dr. Antonia Pajares (Universidad de Extremadura, Spain), Dr. Todora Ivanova Angelova (NTC; Universitat Politécnica de Valéncia, Spain) and Dr. Paul Constantino (St. Michael's College, VT) are gratefully acknowledged. This study was supported by Junta de Extremadura, Spain, and FEDER/ERDF funds (grant IB16139). E. P.-C. gratefully acknowledges support from the Spanish Ministry of Economy and Competitiveness (MINECO) under grant FJCI-2015-27228.

Figure captions

1. Left: schematic of the cyclic, axial contact test. Right: SEM micrograph of the abrasive silica particles used in the tests (in suspension in water, between the sphere and the enamel specimen); note the sharp corners.

2. Optical micrographs showing the scars on enamel occlusal surfaces generated by Hertzian (axial loading) tests in silica particle media, with a sphere of radius 6.35 mm at P=30 N, after (A) 500 cycles, (B) 1000 cycles, (C) 1500 cycles, and (D) 2000 cycles. The contact zones are near circular; dashed lines are a guide for the eyes.

3. Line profiles (horizontal displacement, x; vertical displacement, y) running through the center of scars produced in axial tests after (A) 500 cycles, and (B) 2000 cycles. Note that the scars are relatively shallow, with noisy profiles.

4. Representative SEM micrographs taken from inside scars after axial, cyclic contacts with abrasive particles, showing the damage (pits) on the enamel surface at different magnifications: (A) intermediate; (B) high. Note the high surface roughness, and the limited material removal due to the abrasive particles dislodging material from the surface. White arrows point to relatively large and wide pits, characteristic of a predominantly brittle response; black arrows point to relatively small and sharp pits, characteristic of a predominantly ductile response.

5. (A) Low magnification optical image (stereoscope) of the occlusal surface of an enamel sample after 500 contact cycles; the red and blue arrows indicate the scan

directions in the subsequent OCT analysis. (B) OCT image of the cross-section outside the scar (control). (C) OCT image of the contact cross-section (*i.e.*, under the scar left by the mechanical test); the vertical red arrows mark the diameter of the contact at the occlusal surface, and the black arrows point to the demineralized region (brighter) under the contact.

6. Micrographs of the edge of an axial contact zone/scar (broken white line) after 500 cycles, obtained from (A) 50× optical microscopy, and measurements of the phosphate (PO_4) Raman peak intensities at: (B) 1040±10 cm^{-1}, and (C) 962±10 cm^{-1}.

7. Phosphate (PO_4) Raman spectra collected from inside (red) and outside (blue) an axial scar after 500 cycles. The inset is a zoomed-in view of the (963 ± 3 cm^{-1}) main peak: its intensity is lower inside the scar, indicating demineralization.

8. Set of confocal Raman scans (80 µm x 80 µm) of the Phosphate peak (960 ± 30) cm^{-1} acquired at the edge of a scar after 500 cycles (above) and 2000 cycles (below). Stacks at different depths were performed: for the 500 cycles sample z =0 µm, -2 µm, -4 µm and -6 µm; and for the 2000 cycles sample: z =0 µm, -2 µm, -4 µm and -8 µm. Darker regions correspond to a lower mineral content. Broken white lines mark the edge of the contact zone.

9. (A) Plot of scar volume as a function of number of cycles for cyclic axial contacts with silica abrasives. The line is a linear fit to the data. (B) Comparison between the wear volume of the axial contacts (solid line) and the estimated wear volume produced by an equivalent number of sliding cycles (dashed line), from [12].

References

[1] P.S. Ungar, Teeth: A Very Short Introduction, Oxford University Press, Oxford, UK, 2014.
[2] T.M. Smith, The tales teeth tell, The MIT Press, Cambridge, MA, 2018.
[3] J. Damuth, C.M. Janis, On the relationship between hypsodonty and feeding ecology in ungulate mammals, and its utility in palaeoecology, Biological Reviews 86(3) (2011) 733-758.
[4] A.G. Henry, A.S. Brooks, D.R. Piperno, Microfossils in calculus demonstrate consumption of plants and cooked foods in Neanderthal diets (Shanidar III, Iraq; Spy I and II, Belgium), Proceedings of the National Academy of Sciences of the United States of America 108(2) (2011) 486-491.
[5] O. Borrero-Lopez, A. Pajares, P.J. Constantino, B.R. Lawn, Mechanics of microwear traces in tooth enamel, Acta Biomaterialia 14 (2015) 146-153.
[6] P.J. Constantino, O. Borrero-Lopez, A. Pajares, B.R. Lawn, Simulation of enamel wear for reconstruction of diet and feeding behavior in fossil animals: A micromechanics approach, Bioessays 38(1) (2016) 89-99.
[7] G. Merceron, G. Escarguel, J.M. Angibault, H. Verheyden-Tixier, Can Dental Microwear Textures Record Inter-Individual Dietary Variations?, Plos One 5(3) (2010) e9542 1-9.
[8] M.F. Teaford, P.S. Ungar, Diet and the evolution of the earliest human ancestors, Proceedings of the National Academy of Sciences of the United States of America 97(25) (2000) 13506-13511.
[9] P.S. Ungar, M. Sponheimer, The Diets of Early Hominins, Science 334(6053) (2011) 190-193.
[10] O. Borrero-Lopez, F. Guiberteau, Y. Zhang, B.R. Lawn, Wear of ceramic-based dental materials, Journal of the Mechanical Behavior of Biomedical Materials 92 (2019) 144-151.
[11] O. Borrero-Lopez, A. Pajares, P.J. Constantino, B.R. Lawn, A model for predicting wear rates in tooth enamel, Journal of the Mechanical Behavior of Biomedical Materials 37 (2014) 226-234.
[12] O. Borrero-Lopez, P.J. Constantino, B.R. Lawn, Role of particulate concentration in tooth wear, Journal of the Mechanical Behavior of Biomedical Materials 80 (2018) 77-80.
[13] F. Guiberteau, N.P. Padture, H. Cai, B.R. Lawn, Indentation fatigue - a simple cyclic hertzian test for measuring damage accumulation in polycrystalline ceramics, Philosophical Magazine a-Physics of Condensed Matter Structure Defects and Mechanical Properties 68(5) (1993) 1003-1016.
[14] S. Lathabai, J. Rodel, B.R. Lawn, Cyclic fatigue from frictional degradation at bridging grains in alumina, Journal of the American Ceramic Society 74(6) (1991) 1340-1348.
[15] Y.G. Jung, I.M. Peterson, D.K. Kim, B.R. Lawn, Lifetime-limiting strength degradation from contact fatigue in dental ceramics, Journal of Dental Research 79(2) (2000) 722-731.
[16] Y. Zhang, I. Sailer, B.R. Lawn, Fatigue of dental ceramics, Journal of Dentistry 41(12) (2013) 1135-1147.

[17] N.P. Padture, B.R. Lawn, Contact fatigue of a silicon-carbide with a heterogeneous grain-structure, Journal of the American Ceramic Society 78(6) (1995) 1431-1438.
[18] J.J. Kruzic, J.A. Arsecularatne, C.B. Tanaka, M.J. Hoffman, P.F. Cesar, Recent advances in understanding the fatigue and wear behavior of dental composites and ceramics, Journal of the Mechanical Behavior of Biomedical Materials 88 (2018) 504-533.
[19] Y. Zhang, B.R. Lawn, Evaluating dental zirconia, Dental Materials 35(1) (2019) 15-23.
[20] J.M. Cairney, R. Tsukano, M.J. Hoffman, M. Yang, Degradation of TiN coatings under cyclic loading, Acta Materialia 52(11) (2004) 3229-3237.
[21] R. Ahmed, Contact fatigue failure modes of HVOF coatings, Wear 253(3-4) (2002) 473-487.
[22] Y.F. Jia, F.Z. Xuan, Anisotropic fatigue behavior of human enamel characterized by multi-cycling nanoindentation, Journal of the Mechanical Behavior of Biomedical Materials 16 (2012) 163-168.
[23] S.S. Gao, B.B. An, M. Yahyazadehfar, D. Zhang, D.D. Arola, Contact fatigue of human enamel: Experiments, mechanisms and modeling, Journal of the Mechanical Behavior of Biomedical Materials 60 (2016) 438-450.
[24] Z.H. Xie, E.K. Mahoney, N.M. Kilpatrick, M.V. Swain, M. Hoffman, On the structure-property relationship of sound and hypomineralized enamel, Acta Biomaterialia 3(6) (2007) 865-872.
[25] B.R. Lawn, Indentation of ceramics with spheres: A century after Hertz, Journal of the American Ceramic Society 81(8) (1998) 1977-1994.
[26] M. Machoy, J. Seeliger, L. Szyszka-Sommerfeld, R. Koprowski, T. Gedrange, K. Wozniak, The Use of Optical Coherence Tomography in Dental Diagnostics: A State-of-the-Art Review, Journal of Healthcare Engineering 2017 (2017) 1-31.
[27] Y. Shimada , A. Sadr, Y. Sumi , J. Tagami, Application of Optical Coherence Tomography (OCT) for Diagnosis of Caries, Cracks, and Defects of Restorations, Current Oral Health Reports 2(2) (2015) 73-80.
[28] D.P. Popescu, L.-P.i. Choo-Smith, C. Flueraru, Y. Mao, S. Chang, J. Disano, S. Sherif, M.G. Sowa, Optical coherence tomography: fundamental principles, instrumental designs and biomedical applications, Biophysical reviews 3(3) (2011) 155-169.
[29] I. Ionita, Diagnosis of tooth decay using polarized micro-raman confocal spectroscopy, Romanian Reports in Physics 61(3) (2009) 567-574.
[30] R. Ramakrishnaiah, G.U. Rehman, S. Basavarajappa, A.A. Al Khuraif, B.H. Durgesh, A.S. Khan, I.U. Rehman, Applications of Raman Spectroscopy in Dentistry: Analysis of Tooth Structure, Applied Spectroscopy Reviews 50(4) (2015) 332-350.
[31] L.H. He, M.V. Swain, Understanding the mechanical behaviour of human enamel from its structural and compositional characteristics, Journal of the Mechanical Behavior of Biomedical Materials 1(1) (2008) 18-29.
[32] B. Kerebel, G. Daculsi, L.M. Kerebel, Ultrastructural studies of enamel crystallites, Journal of Dental Research 58 (B) (1979) 844-851.
[33] D. Tabor, The hardness of metals, Oxford University Press, Oxford, UK, 1951.
[34] S.F. Ang, E.L. Bortel, M.V. Swain, A. Klocke, G.A. Schneider, Size-dependent elastic/inelastic behavior of enamel over millimeter and nanometer length scales, Biomaterials 31(7) (2010) 1955-1963.

[35] M. Staines, W.H. Robinson, J.A.A. Hood, Spherical indentation of tooth enamel, Journal of Materials Science 16(9) (1981) 2551-2556.
[36] L.H. He, M.V. Swain, Contact induced deformation of enamel, Applied Physics Letters 90(17) (2007) 171916 1-3.
[37] H.J. Gao, B.H. Ji, I.L. Jager, E. Arzt, P. Fratzl, Materials become insensitive to flaws at nanoscale: Lessons from nature, Proceedings of the National Academy of Sciences of the United States of America 100(10) (2003) 5597-5600.
[38] R. Lewis, R.S. Dwyer-Joyce, Wear of human teeth: a tribological perspective, Proceedings of the Institution of Mechanical Engineers Part J-Journal of Engineering Tribology 219(J1) (2005) 1-18.
[39] F.A. Xhonga, Bruxism and its effect on teeth, Journal of Oral Rehabilitation 4(1) (1977) 65-76.
[40] B.R. Lawn, Fracture of brittle solids, Cambridge University Press, Cambridge,UK, 1993.
[41] P.J. Constantino, O. Borrero-Lopez, B.R. Lawn, Mechanisms of tooth damage and Paranthropus dietary reconstruction, Biosurface and Biotribology 4(3) (2018) 73-78.
[42] F. Santos, A. Branco, M. Polido, A.P. Serro, C.G. Figueiredo-Pina, Comparative study of the wear of the pair human teeth/Vita Enamic (R) vs commonly used dental ceramics through chewing simulation, Journal of the Mechanical Behavior of Biomedical Materials 88 (2018) 251-260.
[43] C. Wulfman, V. Koenig, A.K. Mainjot, Wear measurement of dental tissues and materials in clinical studies: A systematic review, Dental Materials 34(6) (2018) 825-850.

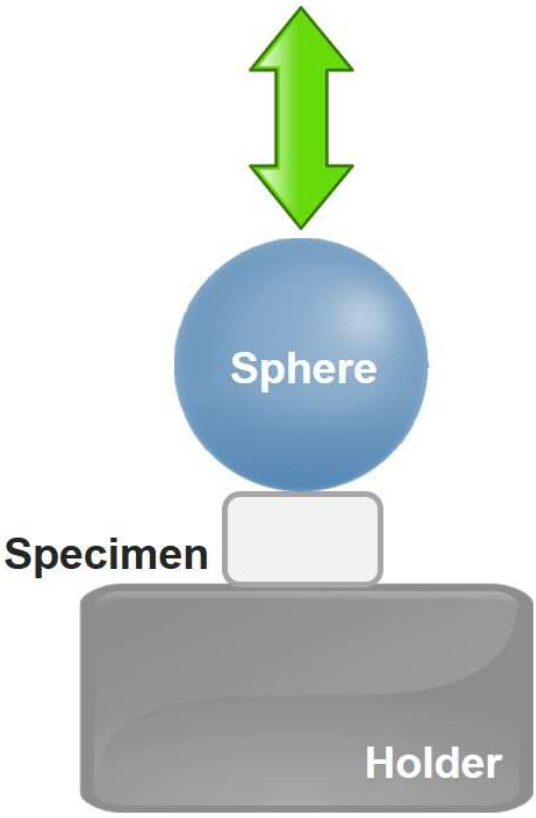

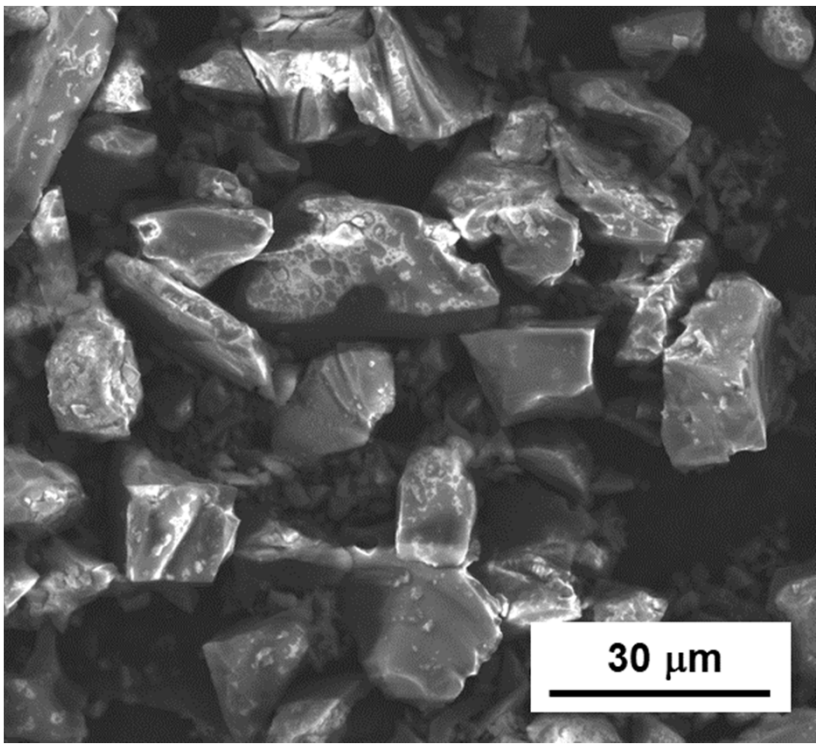

Figure 1

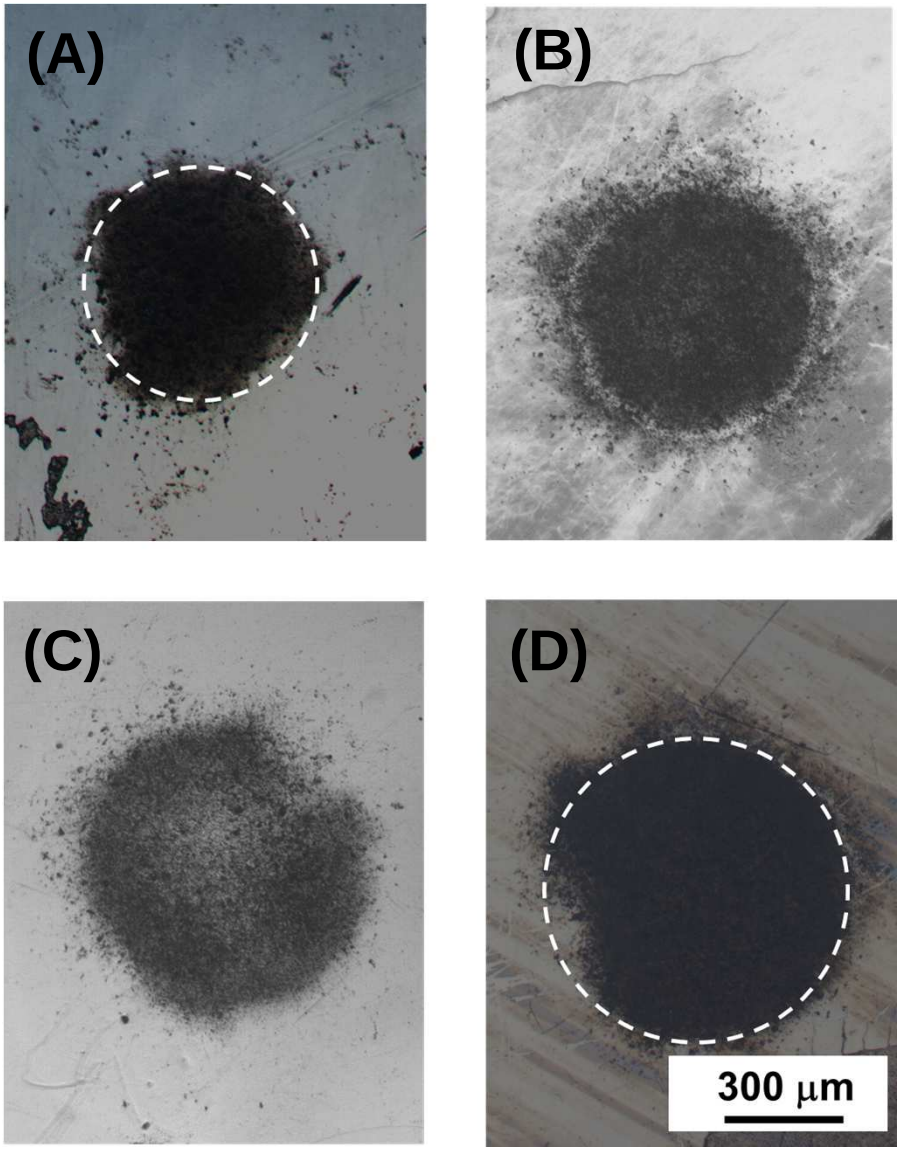

Figure 2

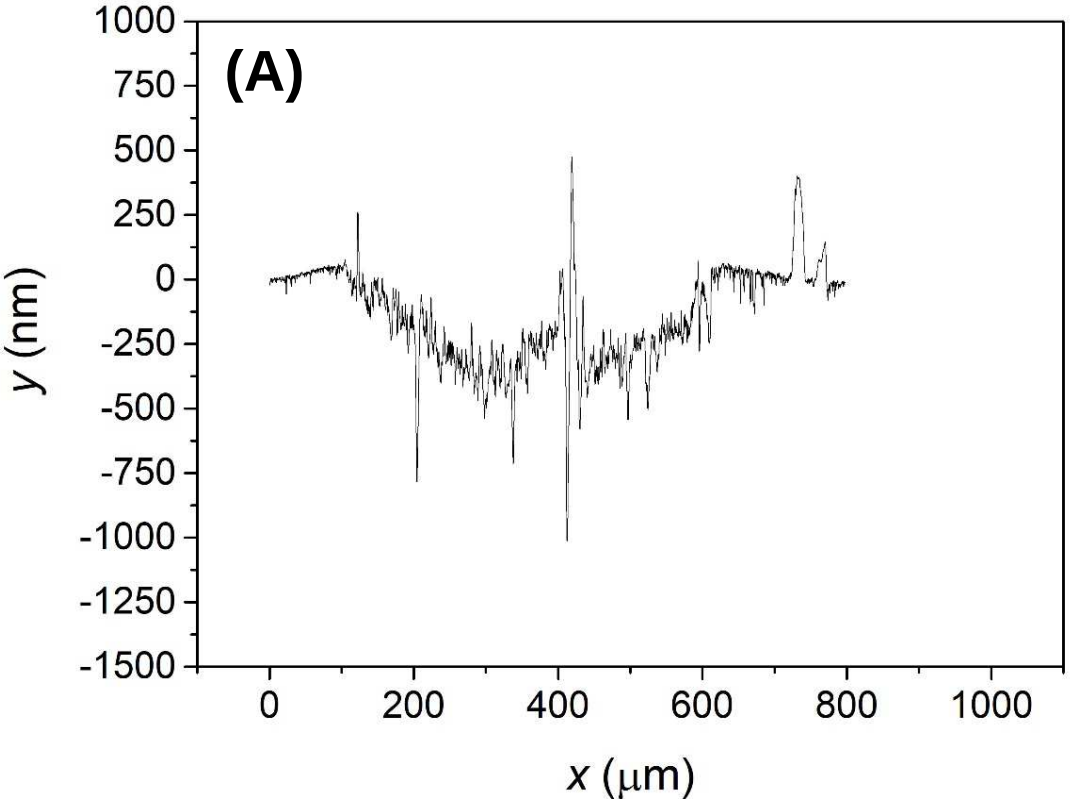
(A)
1000
750
500
250
0
-250
-500
-750
-1000
-1250
-1500
y (nm)
0
200
400
600
800
1000
x (μm)

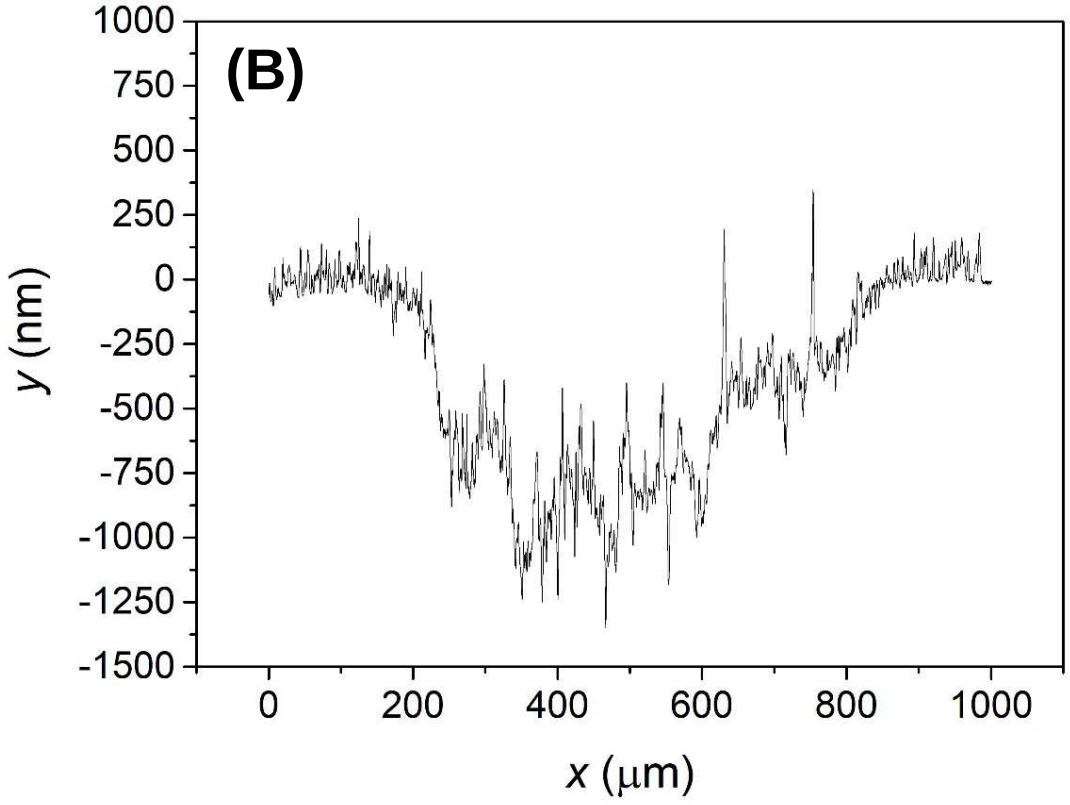
(B)
1000
750
500
250
0
-250
-500
-750
-1000
-1250
-1500
y (nm)
0
200
400
600
800
1000
x (μm)

Figure 3

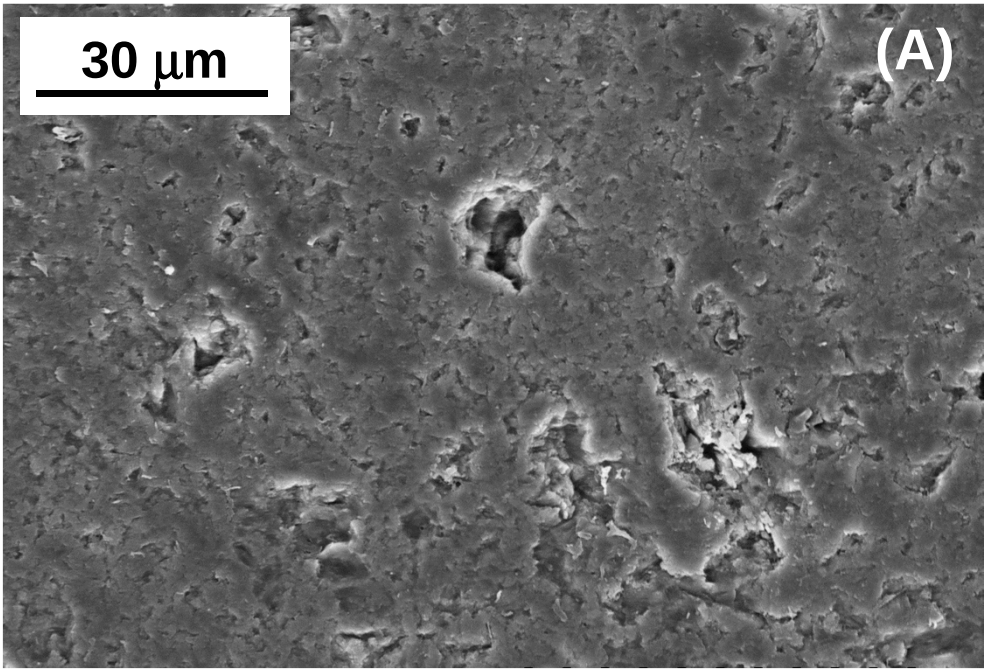

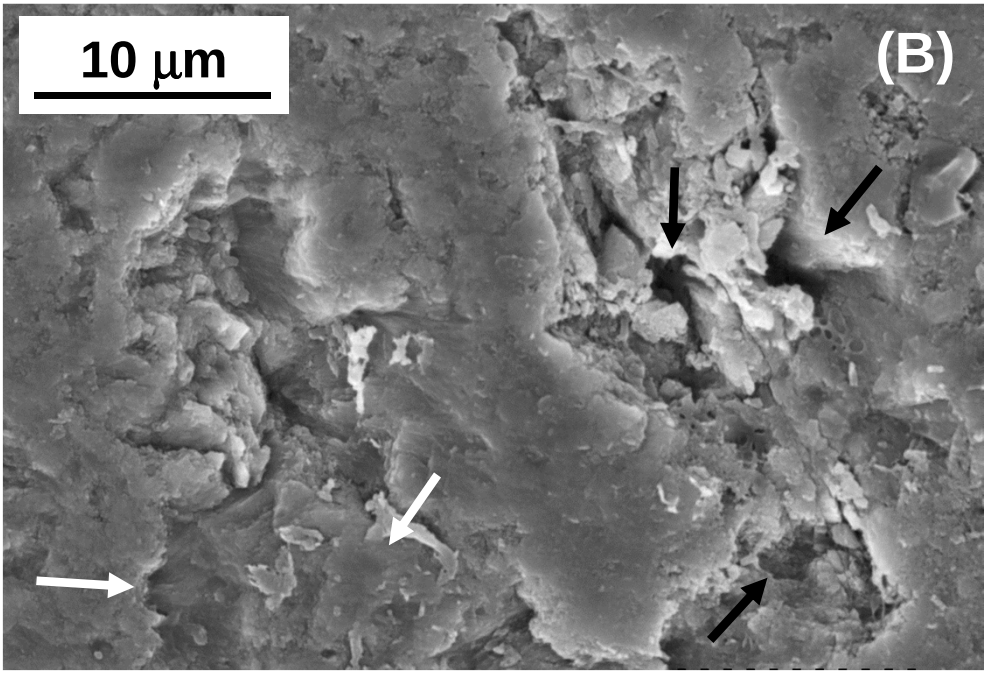

Figure 4

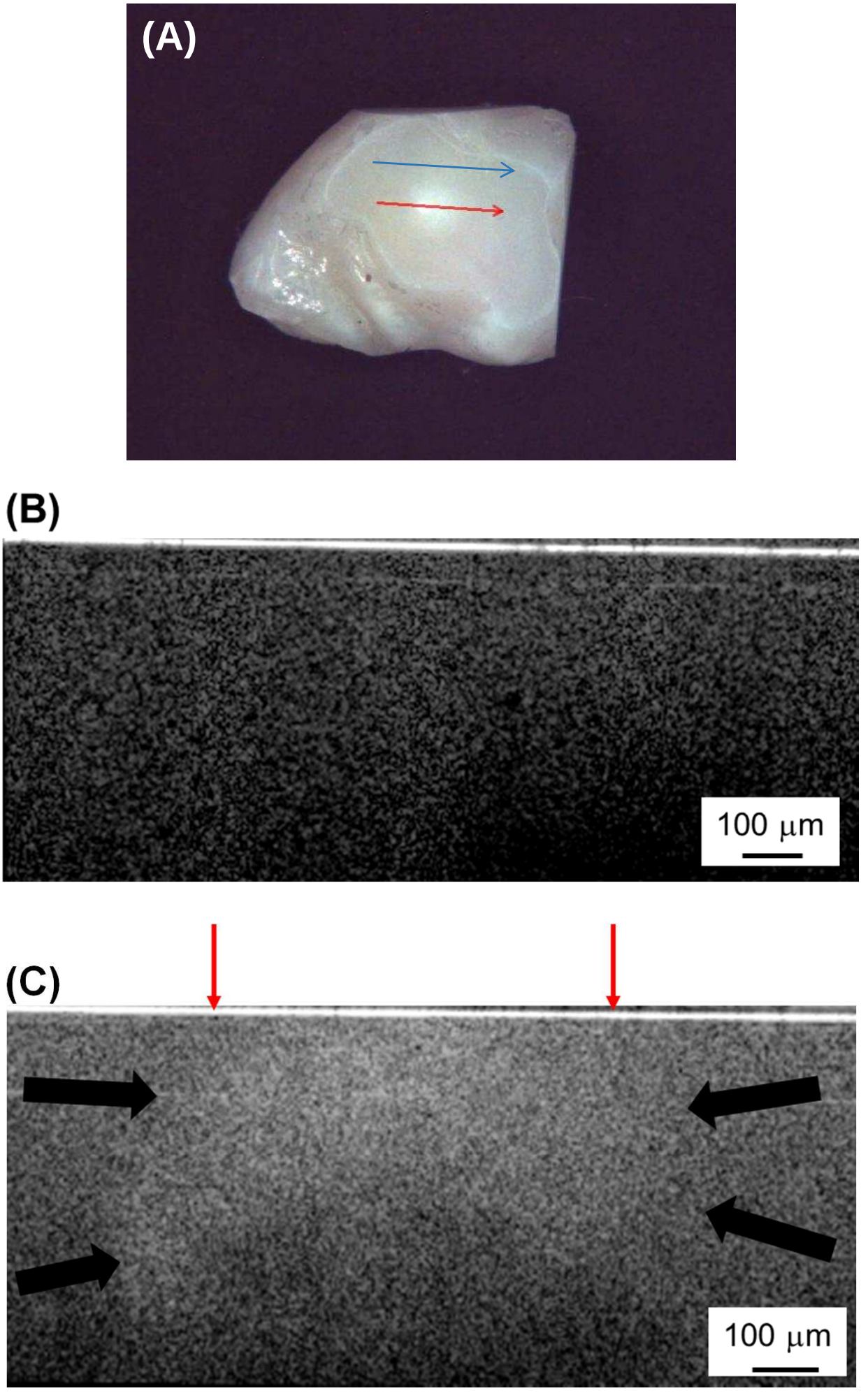

Figure 5

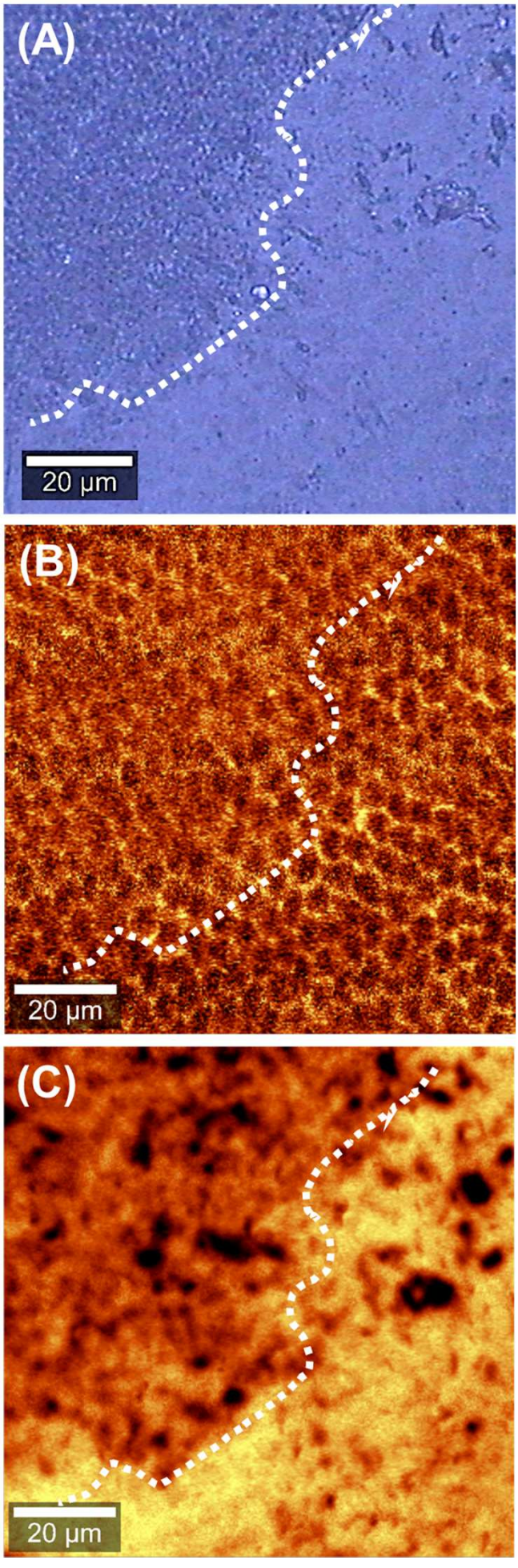

Figure 6

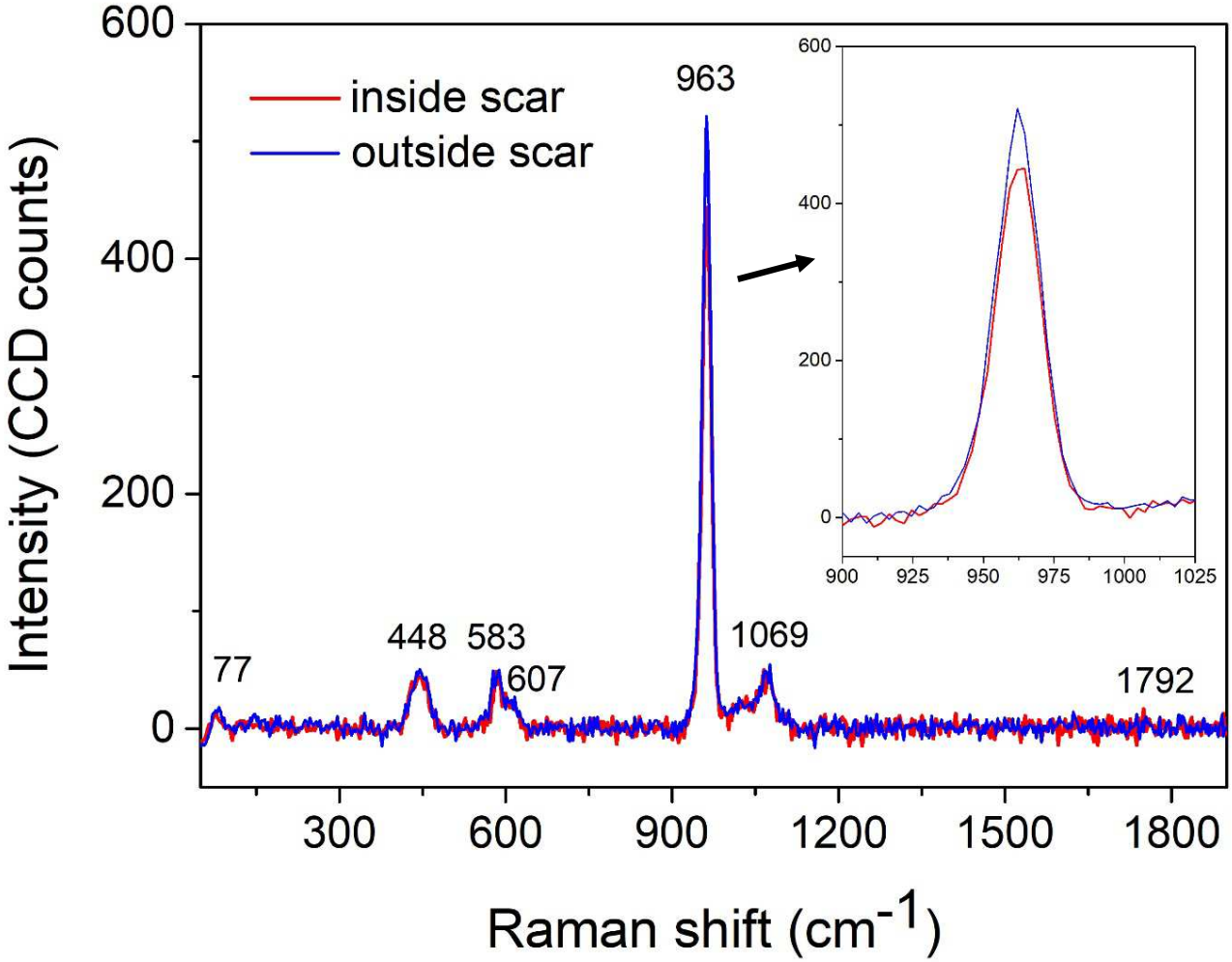
600
400
200
0
Intensity (CCD counts)
inside scar
outside scar
963
448
583
607
77
1069
1792
300
600
900
1200
1500
1800
Raman shift (cm-1)
600
400
200
0
900
925
950
975
1000
1025

Figure 7

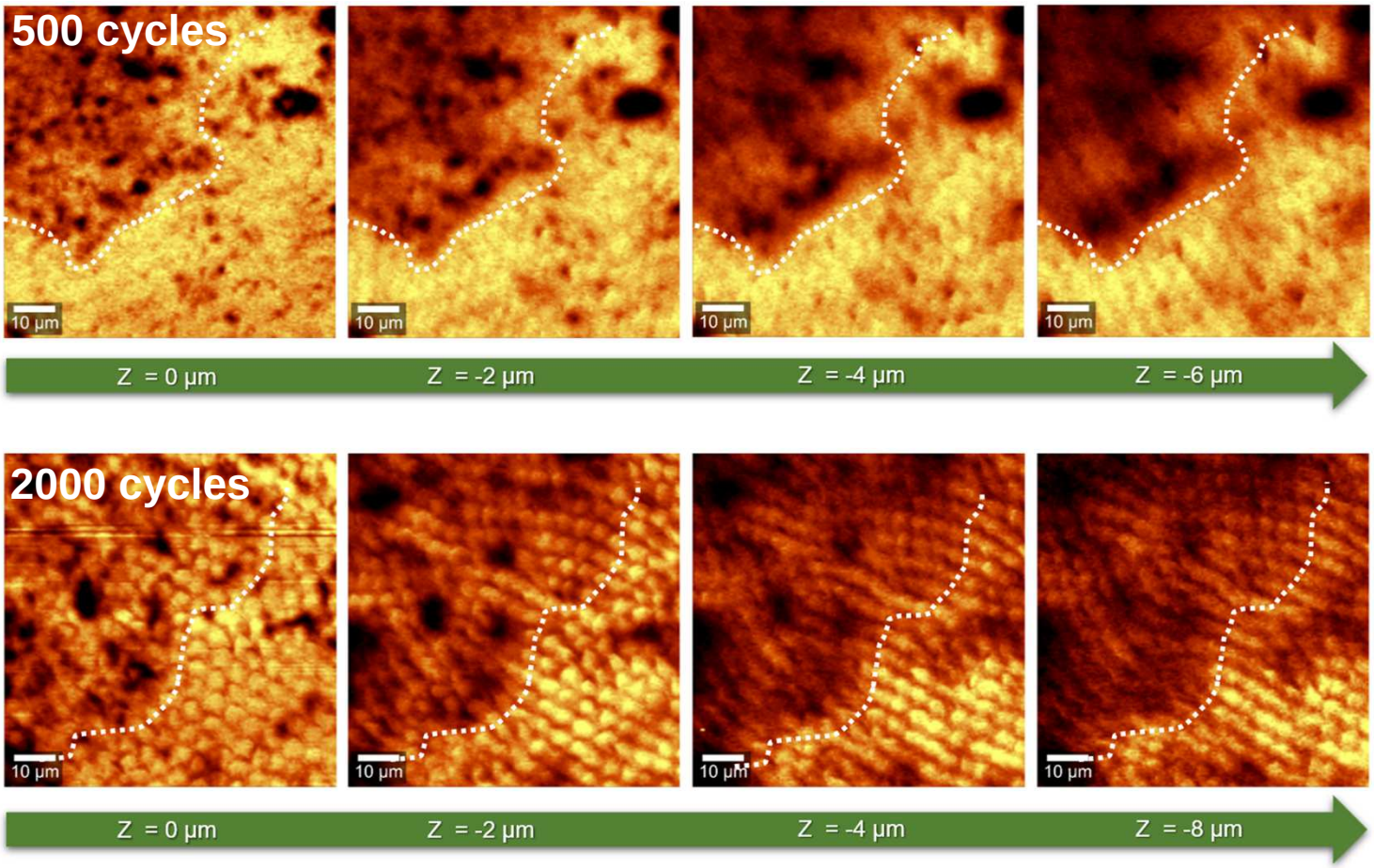
500 cycles
10 µm
10 µm
10 µm
10 µm
Z = 0 µm
Z = -2 µm
Z = -4 µm
Z = -6 µm
2000 cycles
10 µm
10 µm
10 µm
10 µm
Z = 0 µm
Z = -2 µm
Z = -4 µm
Z = -8 µm

Figure 8

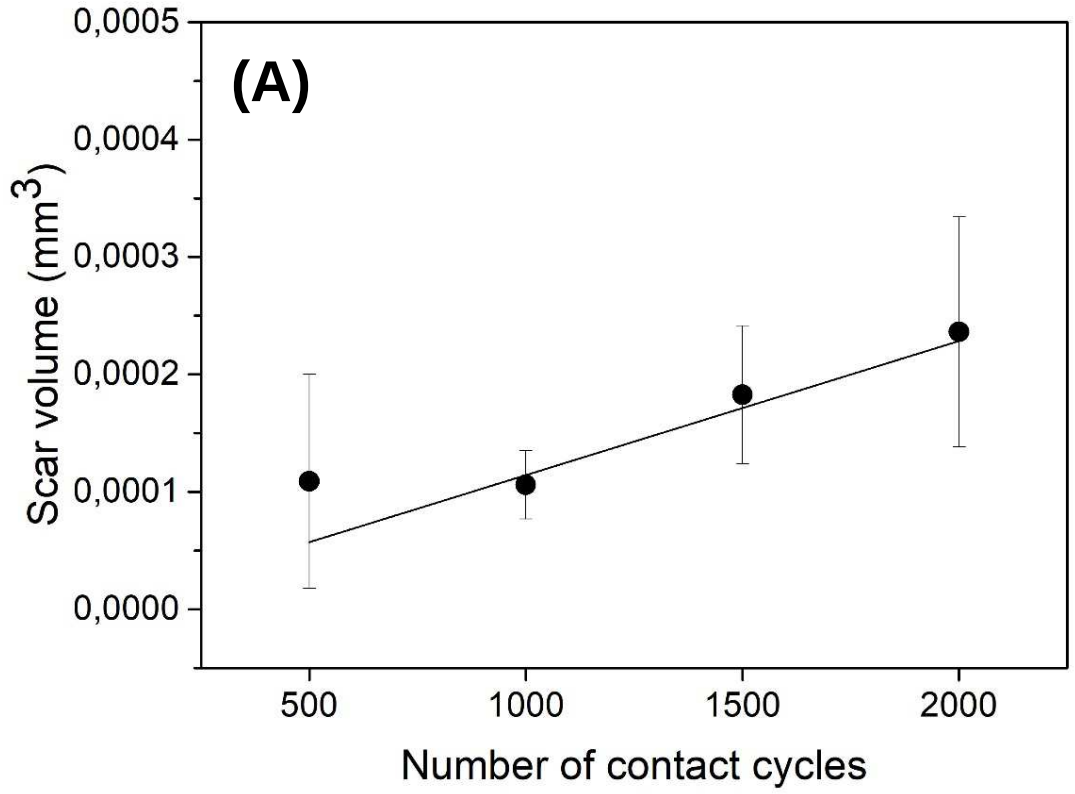
(A)
0,0005
0,0004
0,0003
0,0002
0,0001
0,0000
Scar volume (mm3)
500
1000
1500
2000
Number of contact cycles

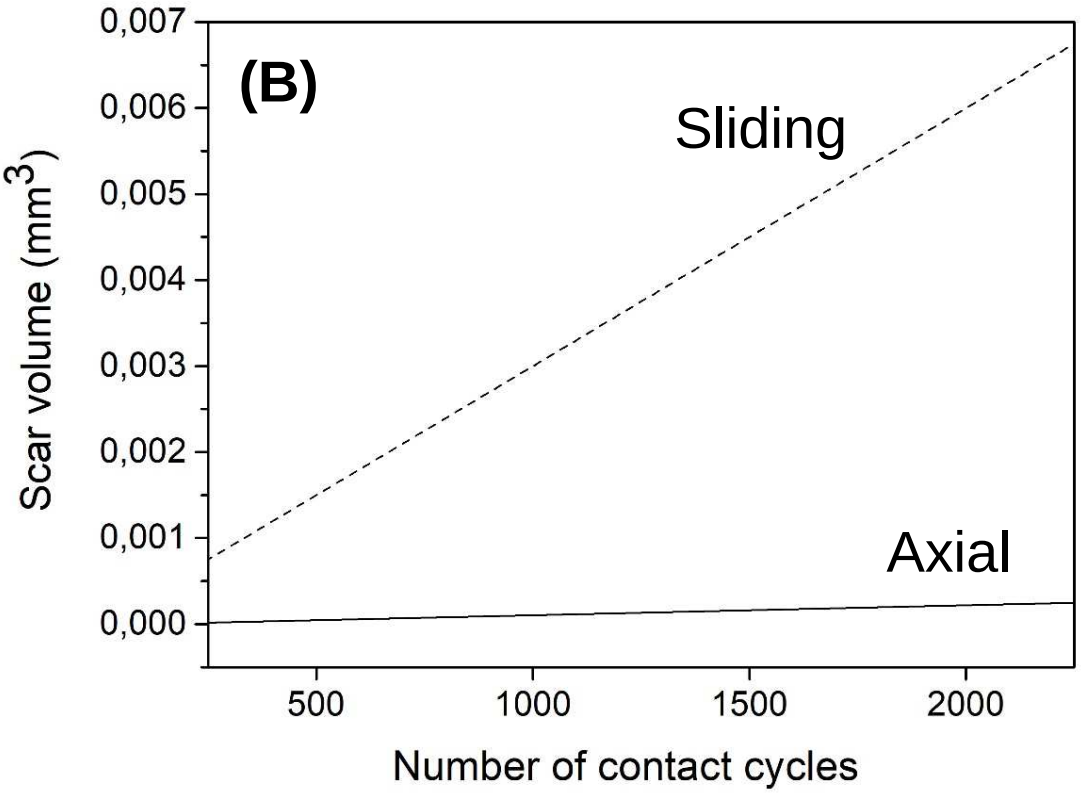
(B)
0,007
0,006
0,005
0,004
0,003
0,002
0,001
0,000
Scar volume (mm3)
Sliding
Axial
500
1000
1500
2000
Number of contact cycles

Figure 9